Geomatics, Natural Hazards and Risk

Monitoring a boreal wildfire using multi-temporal Radarsat-1 intensity and coherence images

Russell Rykhus[a]; Zhong Lu[b]

[a] SGT, contractor to the US Geological Survey (USGS) Earth Resources Observation and Science (EROS) Center, Sioux Falls, SD, USA [b] USGS, EROS Center & Cascades Volcano Observatory, Vancouver, WA, USA

Online publication date: 14 March 2011

PLEASE SCROLL DOWN FOR ARTICLE

Taylor & Francis
Taylor & Francis Group

Monitoring a boreal wildfire using multi-temporal Radarsat-1 intensity and coherence images

RUSSELL RYKHUS*† and ZHONG LU‡

†SGT, contractor to the US Geological Survey (USGS) Earth Resources Observation and Science (EROS) Center, 47914 252nd Street, Sioux Falls, SD 57198, USA
‡USGS, EROS Center & Cascades Volcano Observatory, 1300 SE Cardinal Court, Vancouver, WA 98683, USA

Twenty-five C-band Radarsat-1 synthetic aperture radar (SAR) images acquired from the summer of 2002 to the summer of 2005 are used to map a 2003 boreal wildfire (B346) in the Yukon Flats National Wildlife Refuge, Alaska under conditions of near-persistent cloud cover. Our analysis is primarily based on the 15 SAR scenes acquired during arctic growing seasons. The Radarsat-1 intensity data are used to map the onset and progression of the fire, and interferometric coherence images are used to qualify burn severity and monitor post-fire recovery. We base our analysis of the fire on three test sites, two from within the fire and one unburned site. The B346 fire increased backscattered intensity values for the two burn study sites by approximately 5–6 dB and substantially reduced coherence from background levels of approximately 0.8 in unburned background forested areas to approximately 0.2 in the burned area. Using ancillary vegetation information from the National Land Cover Database (NLCD) and information on burn severity from Normalized Burn Ratio (NBR) data, we conclude that burn site 2 was more severely burned than burn site 1 and that C-band interferometric coherence data are useful for mapping landscape changes due to fire. Differences in burn severity and topography are determined to be the likely reasons for the observed differences in post-fire intensity and coherence trends between burn sites.

1. Introduction

Based on National Interagency Fire Center statistics (http://www.nifc.gov/fire_info/fire_stats.htm), the annual area burned by wildfires in the United States has steadily increased since 1960 and has nationally accelerated by more than 75% (Rykhus 2009) in recent years. A number of factors are thought to have led to the increase: fuel buildup from fire suppression efforts, aging forests, changes in fire policy, expanded public access to and use of forests, and higher temperatures and lower rainfall amounts associated with climate change (http://www.nifc.gov/fire_info/fire_stats.htm; Kasischke and Turetsky 2006). The trend has a profound impact on the overall costs of managing fire-dependent ecosystems and on communities in the wildland–urban interface. The increase in area burned also represents a scientific

*Corresponding author. Email: rykhus@usgs.gov

challenge for restoring impaired ecosystems and assessing positive feedback mechanisms by the release of greenhouse gases in the face of climate change trends. United States national fire management policies, such as the National Fire Plan and the Healthy Forest Restoration Act, call for monitoring capabilities to assess wildland fire trends and provide data for management options and fire science studies. Satellite remote sensing using optical and/or radar sensors is an integral part of the monitoring strategy.

Similar to the conterminous United States, the number of acres burned in Alaska is on the rise, and the state's highest and third highest fire seasons occurred in 2004 and 2005, respectively (Levinson 2004, Kasischke *et al.* 2007). During the 2004 Alaska fire season, about 2.7 million hectares of forests were consumed by wildland fires. This increase in burned area is consistent with that observed throughout the North American boreal forest region (Gillett *et al.* 2004, Kasischke *et al.* 2007) and may be related to recent climate warming (Kasischke and Turetsky 2006, O'Neal *et al.* 2006). Also, the increase in acreage burned appears to be accompanied by an increase in the number of large boreal forest fires (Levinson 2004). Boreal wildfires are a natural part of the ecosystem and play an important role in maintaining and regenerating fire-dependent ecosystems. Fire is important for boreal ecological processes because the depth of the top-most organic soil layer (duff layer) controls tree recruitment and vegetation recovery (Landhausser and Wein 1993, Johnstone and Chapin 2006).

The objective of this paper is twofold. First, we analyse the ability of C-band HH-polarization Radarsat-1 intensity data to monitor changes to the boreal vegetation caused by wildfires. Second, we seek to examine the utility of the phase portion of the radar signal to monitor during-fire and post-fire vegetation changes by using interferometric coherence images. Using multi-temporal Radarsat-1 data for the 2003 B346 fire, we propose to (a) monitor the fire's effect on the backscattered intensity signal while the fire was actively burning and during the post-fire analysis, (b) use the intensity and coherence data to determine burn severity at the two burned sites, and (c) use coherence data to monitor the temporal trends during-fire effects on the landscape and post-fire vegetation recovery.

2. Background

2.1 *Fire studies: synthetic aperture radar*

A significant body of research using various synthetic aperture radar (SAR) systems has been applied to mapping fires in boreal forests (Kasischke and French 1995, Bourgeau-Chavez *et al.* 1997, French *et al.* 1999, Bourgeau-Chavez *et al.* 2002). Synthetic aperture radar data are sensitive to changes in surface roughness and the dielectric constant, which is primarily controlled by the moisture characteristics of the soil and vegetation (Ulaby *et al.* 1986, Dobson *et al.* 1995, Henderson and Lewis 1998). Radar-based wildfire studies of boreal forests typically use C-band radar systems because the approximately 5.6 cm wavelength is well-suited to the structure of the boreal ecosystem vegetation (Bourgeau-Chavez *et al.* 1997). Thus, wildfire-induced changes in the boreal forests may go largely undetected using longer L-band (about 24-cm wavelength) radar systems (Bourgeau-Chavez *et al.* 1997). Studies have found that the burning of boreal vegetation will typically lead to increased backscattered values for both the European Resources System (ERS-1) and the

Radarsat-1 system (Bourgeau-Chavez *et al.* 1997). Bourgeau-Chavez *et al.* (1997) concluded that higher than normal backscatter returns were due to post-fire increases in soil moisture, surface roughness, and the burning of leaves, all of which cause an increase in the number of double-bounce interactions. A wildfire study conducted using both ERS-2 and Radarsat-1, beam mode 1 and beam mode 7 data revealed that the strength of the intensity return is also dependent on the incidence angle (beam mode) used during acquisition (French *et al.* 1999). The backscatter return for the Radarsat-1, beam mode 1 (with an incidence angle similar to ERS-1/2) scene exhibited higher than background intensity levels within the burned area, while the intensity return for the Radarsat-1, beam mode 7 scene, with a higher incidence angle of about 40° exhibited lower than normal intensity levels within the burned area (French *et al.* 1999).

Recent C-band SAR studies of boreal wildfires use the intensity data to monitor an area's susceptibility to wildfire. This is accomplished by monitoring the spatial variation of soil moisture within a previously burned area. Soil moisture information is then combined with fire weather index data provided with the Canadian Forest Fire Danger Rating System to classify fire risk (Bourgeau-Chavez *et al.* 1999, Leblon *et al.* 2002, Abbott *et al.* 2007). According to these studies, low backscatter values within an older burn area indicate low soil moisture levels. Areas outside the burned forest with similar backscatter values are also interpreted as dry and thus more likely to have a fire (Bourgeau-Chavez *et al.* 1999). Studies conducted by both Leblon *et al.* (2002), who used ERS-1 data and Abbott *et al.* (2007), who used Radarsat-1 data, obtained high R^2 values between the backscattered value and the duff moisture code, drought code and build-up index used by the Canadian Forest Fire Danger Rating System. Soil moisture not only influences the amount of the backscattered SAR signal but also relates to the depth of the remaining duff layer, which in turn plays an important role in vegetation regrowth. According to the authors, soil moisture is positively related to the depth of the duff layer and duff layers greater than about 7 cm lead to higher soil moisture levels (Kasischke and Johnstone 2005, Bourgeau-Chavez *et al.* 2007). Increased moisture and thickness of the duff layer in turn affect vegetation recruitment in recently burned areas (Johnstone and Chapin 2006). Thus, C-band radar provides not only information on post-burn vegetation structure but also information relating to soil moisture within a burned area as dictated by the dielectric constant of the vegetation and soil.

2.2 *The study area*

For this research, we chose to study a 2003 wildfire (centred at N66° 53′ 39″ and W147° 25′ 28″) in the Yukon Flats National Wildlife Refuge, Alaska (figure 1). The 2003 wildfire, named B346 (figure 1) by the Alaska Fire Service, started in the foothills of the Philip Smith Mountains. According to a GIS database developed by the Bureau of Land Management, Alaska Fire Service (http://agdc.usgs.gov/ data/blm/fire), the B346 fire consumed about 84 000 ha of boreal forest. The Yukon Flats physiographic region contains one of Alaska's most extreme fire climates because of the low precipitation and relatively high summer temperatures (Bonan and Shugart 1989). According to the National Elevation Dataset (NED) digital elevation data (DEM) developed by the US Geological Survey (USGS) (Gesch 1994), the greater study area ranges in elevation from about 50 m in the southeast to about 1000 m in the northwestern part of the study area (figures 1 and

2(*a*)). While the extreme northwestern portion of the study area has a significant amount of slope, the majority of the B346 fire site is located on gently rolling hills (figures 1 and 2(*a*)).
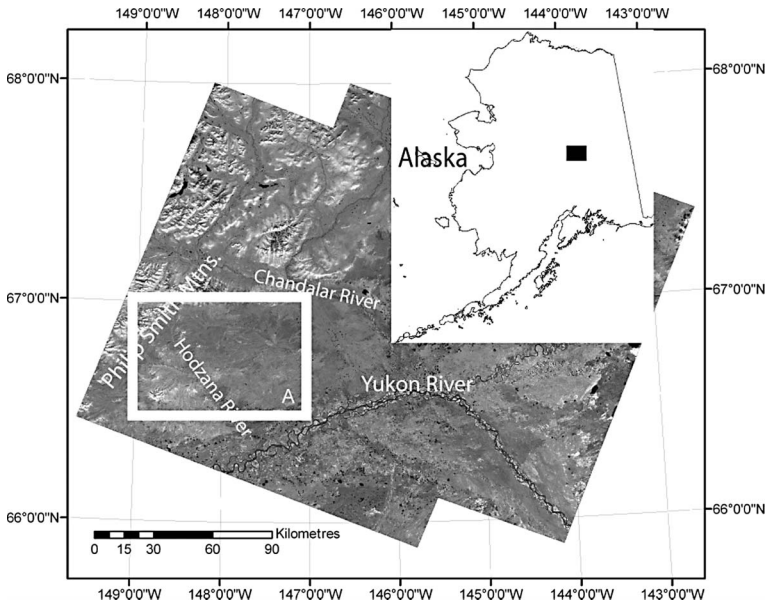
Figure 1.   Approximate location of the B346 wildfire (white box); some prominent features located near the burned area are identified.
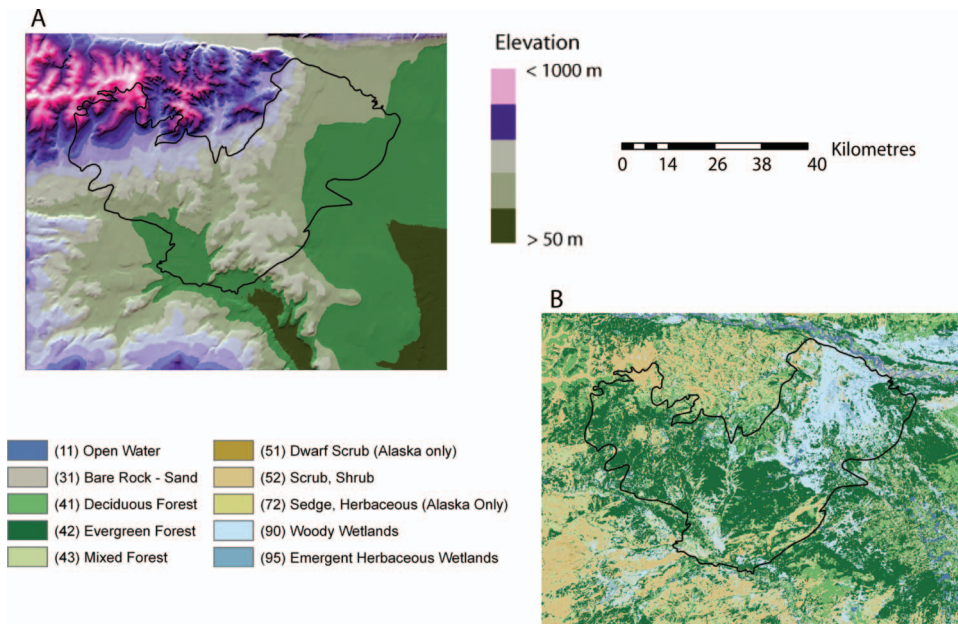

Figure 2.   Painted relief of the topography found within the greater B346 area (A). The National Land Cover Database 2001 and modified Anderson Level II classification scheme (B) are presented.

2.3 *The SAR signal*

A SAR system transmits and receives electromagnetic waves at wavelengths ranging from a few millimetres to tens of centimetres. The emitted radar wave is propagated through the atmosphere until it contacts the Earth's surface. Part of the emitted wave is then returned to and recorded by the SAR sensor. The SAR signal contains information not only on the intensity of the returned wave but also on the phase of the returned wave. Using sophisticated image processing techniques called SAR processing (Curlander and McDonough 1991, Bamler and Hartl 1998, Henderson and Lewis 1998), both the intensity and phase of the reflected (or backscattered) signal of each ground resolution element (a few metres to tens of metres) can be calculated in the form of a complex-valued SAR image. The intensity of the returned SAR signal is primarily controlled by surface roughness, terrain slope, and dielectric constant. While the dielectric constant is primarily determined by the amount of water found in the soil and/or vegetation. The phase portion of the SAR signal is controlled primarily by the distance between the satellite antenna and ground targets, atmospheric delays, and the interaction of the electromagnetic wave with ground surface targets.

When the radar wave contacts a vegetated surface, three types of interactions can occur: (1) surface scattering, (2) volume scattering, and (3) double-bounce (Dobson *et al*. 1995, Henderson and Lewis 1998). Surface scattering is the interaction between a surface and the radar wave and is controlled by surface roughness, dielectric constant (moisture content of the soil and plant materials) and terrain slope. If the surface is smooth with respect to the radar's wavelength, the signal is reflected directly away from the sensor (specular reflection), resulting in very low backscatter return. With volume scattering, the radar wave makes contact with the vegetation canopy, which has many scattering elements and reflects the SAR signal in all directions, resulting in a moderate backscatter return. Penetration of the vegetation canopy is dependent on several factors, including the wavelength of the SAR system, canopy density and leaf size. However, if the SAR signal can penetrate the vegetation canopy, a double-bounce interaction may occur. Double-bounce interactions typically occur in urban areas and flooded forests (Lu *et al*. 2005a, Kwoun *et al*. 2006). For example, when the radar wave penetrates the vegetation canopy of a flooded forest, it will make contact with the bole of the tree, be directed downwards towards the water's specular surface, and then be reflected directly back towards the sensor. The double-bounce interaction, therefore, results in very high or bright radar intensity returns.

2.4 *The coherence signal*

Interferometric SAR (InSAR) is a technique used to map surface deformation caused by a variety of both natural and anthropogenic sources. The primary output of InSAR is an interferogram that depicts the amount and extent of the surface deformation. It is a common practice during InSAR processing to create a coherence image that measures the degree of correlation between two SAR images acquired at different times. As a by-product of InSAR processing, the coherence image is used to qualitatively assess the changes or modifications in radar backscattering signal. Higher coherence values indicate that the backscattering elements within the resolution cell remain relatively unchanged or undisturbed at

the scale of the SAR wavelength over the observation period. In theory, an interferogram and coherence images can be generated for all possible interferometric pairs. However, orbital geometric and temporal constraints restrict the total number of viable coherence pairs (Zebker and Villasenor 1992). For example, if the baseline (the spatial distance between two orbits at the time the images are acquired) or if the temporal separation between image acquisitions is too large, the coherence values become meaningless. In InSAR, coherence is typically calculated using both the intensity and phase information from the scenes. Since changes to the structure of the vegetation can be measured using the intensity part of the returned radar signal, we calculated the coherence using only the phase portion of the radar signal. This way the coherence data become more sensitive to changes to the height of the vegetation.

With InSAR, loss of coherence is a bad thing and is typically referred to as decorrelation. There are three primary types of decorrelation: (a) thermal decorrelation, caused by uncorrelated noise sources within the radar instruments, (b) spatial decorrelation, caused by viewing the target from different locations in space, and (c) temporal decorrelation, typically caused by environmental changes (Henderson and Lewis 1998, Lu *et al.* 2005a,b, Lu *et al.* 2007). The environmental changes that can cause temporal decorrelation include vegetation growth, the erosion/deposition of surface materials, dense vegetation, the presence of ice/snow, winds sufficient to move the vegetation canopy, and the diurnal freezing/thawing and subsequent refreezing of surface materials (Wegmuller 1990, Hagberg *et al.* 1995, Kasischke and Johnstone 2005, Ramsey *et al.* 2006). For very dense forests, a C-band Radarsat-1 system may completely lose coherence over even the shortest observation periods (24 days for Radarsat-1). However, if the SAR signal can penetrate the vegetation canopy, such as with moderately dense boreal forests, and if the soil is moist, the signal should remain coherent between short observation periods. Under most conditions, standing water will lead to a total loss of coherence (Dobson *et al.* 1995, Henderson and Lewis 1998). Even though the loss of coherence in InSAR studies is problematic for deformation mapping, the loss of coherence caused by a wildfire may yield information useful for mapping vegetation damage, fire severity, and/or post-fire vegetation recruitment. The coherence estimates only provide a snapshot of how the surface changed with respect to the vegetation structure between the two SAR acquisitions.

3. Data

3.1 *Radarsat-1 data*

The Radarsat-1 sensor, operated by the Canadian Space Agency (CSA), has a C-band wavelength (~ 5.7 cm), HH polarization, a 24-day repeat-pass frequency, and the capability of acquiring data with incidence angles ranging from $\sim 23°$ to $\sim 49°$. The Radarsat-1 scenes over the 2003 B346 fire were all acquired during ascending passes with an incidence angle of about $23°$ (standard beam mode 1) at about 7:00 pm local time the previous day. Information relating to the individual Radarsat-1 scenes used in this study is provided in table 1 and baseline temporal separation of the coherence images can be found in table 2.

The GAMMA$^{©}$ SAR processing software was used to process the raw (Level 0) Radarsat-1 data into a single look complex image containing information on both

Table 1. List of C-band Radarsat-1 SAR imagery used in the analysis of the B346 Alaskan wildfire and the corresponding location where the images are displayed.

	Date of acquisition (mm/dd/yyyy)	Figure
1	07/05/2002	Figure 5
2	07/29/2002	Figure 5
3	08/22/2002	Figure 5
4	09/15/2002	Figure 5
5	04/19/2003	Not Shown
6	05/13/2003	Not Shown
7	06/06/2003	Not Shown
8	06/30/2003	Figure 5
9	07/24/2003	Figures 4 & 5
10	08/17/2003	Figures 4 & 5
11	09/10/2003	Figures 4 & 5
12	10/04/2003	Figures 4 & 5
13	12/15/2003	Figure 5
14	01/08/2004	Not Shown
15	05/07/2004	Figure 5
16	05/31/2004	Figure 5
17	06/24/2004	Figure 5
18	07/18/2004	Figure 5
19	08/11/2004	Figure 5
20	09/04/2004	Figure 5
21	05/02/2005	Figure 5
22	06/19/2005	Figure 5
23	07/13/2005	Figure 5
24	08/06/2005	Figure 5
25	08/30/2005	Figure 5

Table 2. List of all C-band Radarsat-1 coherence pairs with a temporal change of less than 1 year and the baseline estimate for that pair. Large baselines, Doppler shifts, temporal differences, and other orbital geometry issues precluded the calculation and use of all possible interferometric coherence estimates. The changes depicted in the individual coherence pairs represent a snapshot of a continuously changing landscape.

Reference image (mm/dd/yyyy)	Subordinate image (mm/dd/yyyy)	Delta (Δ) days	Perpendicular baseline (m)	Figure
07/29/2002	08/22/2002	24	110	Figure 7(a)
07/29/2002	09/15/2002	48	-400	Figure 7(b)
06/30/2003	07/24/2003	24	-174	Figure 7(c)
07/24/2003	08/17/2003	24	-32	Figure 7(d)
08/17/2003	09/10/2003	24	397	Figure 7(e)
08/17/2003	10/04/2003	48	-267	Figure 7(f)
06/24/2004	07/18/2004	24	42	Figure 7(g)
06/24/2004	08/11/2004	48	-91	Figure 7(h)
06/24/2004	09/04/2004	72	67	Figure 7(i)
07/18/2004	08/11/2004	24	-134	Figure 7(j)
07/18/2004	09/04/2004	48	24	Figure 7(k)
08/11/2004	09/04/2004	24	158	Figure 7(l)
06/19/2005	08/06/2005	48	-65	Figure 7(m)
08/06/2005	08/30/2005	24	-11	Figure 7(n)

the phase and intensity of the SAR backscatter signal. During SAR processing, the 15-minute USGS NED digital elevation model (DEM) (Gesch 1994), with a specified horizontal accuracy of ~60 m, root-mean-square vertical error of less than 15 m, and a horizontal resolution of 90 m, was used to reduce topographic effects in both the intensity and phase data (Massonnet and Feigl 1998). The NED dataset was subsequently used to convert the intensity and coherence images in SAR coordinates to the UTM projection coordinate system. During SAR processing, we applied a speckle suppression algorithm to the individual scenes (Lee 1986). After geo-registration, the linear intensity values were converted to decibel power scale.

3.2 *The land-cover data*

As previously indicated, the interaction between C-band HH polarized SAR and vegetation is determined mainly by vegetation structure and dielectric constant. So how can the type of interaction for a particular type of vegetation be determined? Normally, this is accomplished using field data containing information not only on the land cover type but also on the percent of canopy closure, vegetation height, biomass, etc. While we do not have any pre- or post-fire field data for the B346 fire, we have used the National Land Cover Dataset (NLCD) (figure 2(*b*)) developed by the US Geological Survey (USGS), as a surrogate for field data depicting pre-fire vegetation conditions. The NLCD was created using 2001 era Landsat 5 and Landsat 7 imagery (Vogelman *et al.* 2001, Homer *et al.* 2004, 2007) using a slightly modified Anderson level II classification scheme with a semi-automated methodology and consistent data sources. Thus, the NLCD has a nominal ground resolution of 30 m. The Landsat Enhanced Thematic Mapper Plus (ETM+) imagery were acquired prior to the B346 fire and before the advent of the Scan Line Corrector problem. Because of Alaska's unique types of vegetation, additional classes were added to the NLCD classification scheme. According to the NLCD database for the greater study area, the site is dominated by Evergreen Forests, Mixed Forests, and Woody Wetlands. Figure 2(*b*) shows the spatial distribution of the NLCD-derived land cover classes.

3.3 *Normalized Burn Ratio data*

For the B346 fire, we downloaded all available Normalized Burn Ratio (NBR) images that were originally processed for the USGS Landfire Program from the USGS GloVis website (http:/glovis.usgs.gov). The package downloaded not only includes an NBR image but also the six Landsat Thematic Mapper (TM)/ETM+ reflectance bands, a 3-band tasseled cap transformation, two thermal bands, and when available, the pan band (i.e. when the Landsat ETM+ sensor was used). From GloVis we have acquired four NBR images acquired on 16 August 2000, 22 August 2002, 14 August 2005 and 28 August 2007 (figure 3). The 16 August 2000, 22 August 2002, and 14 August 2005 images were acquired using the Landsat ETM+ sensor, and the 28 August 2007 image was acquired by the Landsat TM sensor (figure 3). Stripes of missing data in the 14 August 2005 scene are caused by the failure of the Scan Line Corrector onboard the Landsat 7 sensor (figure 3(*c*)). Fortunately, the B346 fire was located near the centre of the 14 August 2005 scene, minimizing the amount of lost data.
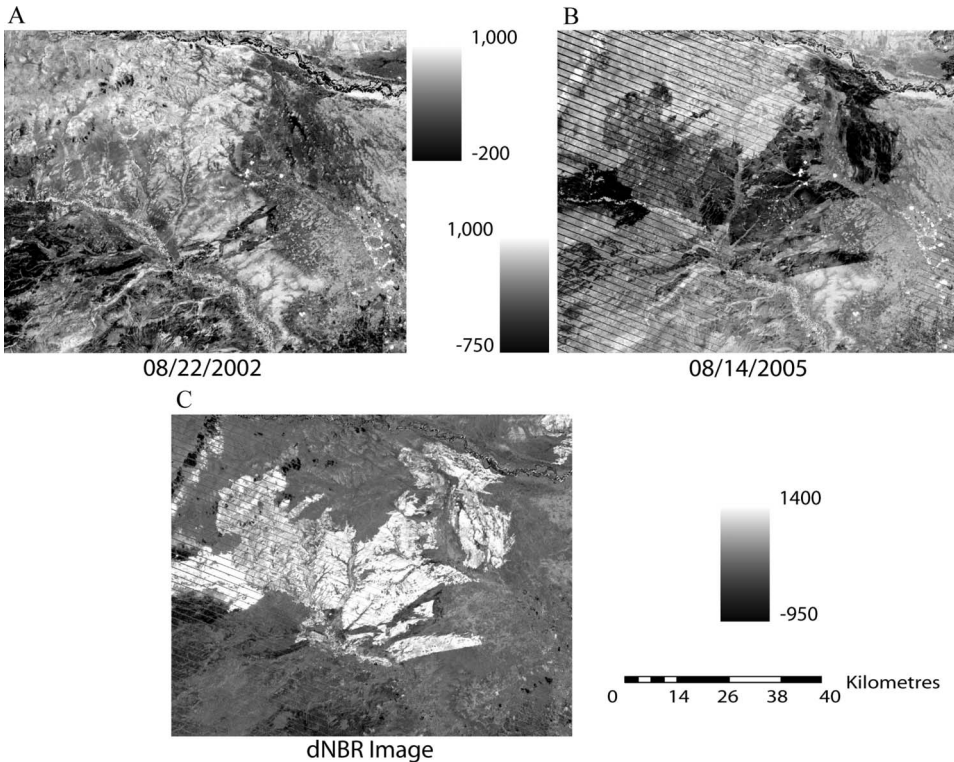
Figure 3. Available Normalized Burn Ratio (NBR) information derived from the Landsat ETM+ sensor for the B346 fire (A & B). Difference NBR (dNBR) image created from the 22 August 2002 and the 14 August 2005 NBR images (C). Unfortunately, no 2004 NBR data were available. The NBR data are available free of charge via the USGS GloVis website. The stripes of missing data in the 14 August 2005 data are due to the failure of the Scan Line Corrector on board the Landsat ETM+ sensor during the spring of 2003. The pre-fire NBR image (A) has the narrowest range of values while the largest range is found in the difference (C) image.

The NBR is a ratio of the near-infrared (Landsat ETM+ band 4) and mid-infrared (Landsat ETM+ band 7) portions of the electromagnetic spectrum and is calculated as follows:

$$NBR = 1000[(band4 - band7)/(band4 + band7)] \qquad (1)$$

The NBR index was calculated using at-satellite reflectance data and was converted by the USGS to a signed 16-bit image, significantly reducing the size of the files (figure 3(*a*) and (*c*)). Burned areas in an NBR image typically appear much darker than the surrounding unburned forests. However, studies using NBR data to estimate burn severity do not typically use the NBR per-pixel value; instead, they create an NBR difference image by subtracting the post-fire image from the pre-fire image (Key and Benson 2006, Lutes *et al.* 2006). This image is referred to as the differenced Normalized Burn Ratio (dNBR) data. Subtracting the post-fire NBR image from a pre-fire NBR image, burned areas appear in bright tones and the surrounding unburned forests appear in various grey tones. For this study, we

differenced the 22 August 2002 and the 14 August 2005 NBR images. The 3-year temporal separation is not optimal, but the data should still provide a relatively accurate spatial representation of burn severity of the B346 fire as the vegetation at this latitude grows quite slowly.

4. Analysis and discussion

To measure the spatial and temporal characteristics of the B346 fire, we decided to subset three 30 by 30 pixel areas. Two of the study sites were selected from within the fire, and the third site was taken from nearby unburned boreal forests (figure 4(*d*)). The two sites within the B346 area were chosen because of their relatively homogeneous nature and differences in both topography and temporal evolution of the fire (figures 2(*a*) and 4(*d*)). For each 30 by 30 pixel chip, we calculated the average and standard deviation statistics for each Radarsat-1 backscatter intensity and InSAR coherence image (figure 4(*d*)). Most subsequent power values are mean values calculated for their respective study site and are accompanied by the standard deviations (SD).
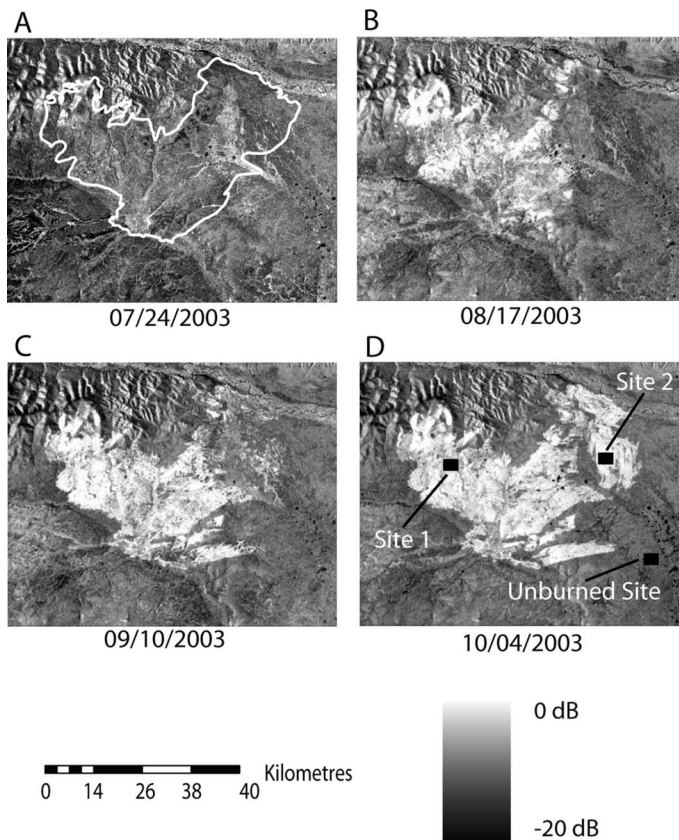

Figure 4. Radarsat-1 intensity data for the B346 fire acquired shortly after the fire started (A) and while the fire was actively burning (B, C, and D). Burning of the boreal vegetation caused an increase in the backscattered intensity return. The three study sites referred to in the text are identified in the 4 October 2003 image.

4.1 Analysis of pre- and during-fire data

Prior to the acquisition of the 24 July 2003 radar image, the backscattered intensity levels for all three study sites were within about 2 dB of each other at about –11 dB (figure 5(*a*)–(*f*) and figure 6(*a*)). With the acquisition of the 17 August 2003 Radarsat-1 image, the backscattered intensity levels for burn site 1 suddenly increased to about -7 dB (± 1.3 SD), but the backscattered values for the other two test sites remained at near normal levels (figure 6(*a*), line a). Close visual examination of the 24 July 2003 intensity image revealed many clusters with very bright or high radar returns (figure 4(*a*)). By the acquisition of the 4 October 2003 image, the fire had progressed eastwards towards burn site 2 (figure 4). For the 4 October 2003 scene, the intensity values for burn site 1 had climbed to -4 dB (± 1.03 SD), and burn site 2 was also very bright at -4 dB (± 1.02 SD) (figure 6(*a*), line b). The B346 fire caused an increase in intensity values of about 6 to 7 dB over pre-fire intensity levels.

Examination of the pre-fire coherence profiles in figure 6(*b*) shows that all three test sites were very coherent with values of about 0.8 and varying by only 0.1. The sudden jump in intensity values brought about by the fire was accompanied by an equally drastic drop in coherence (figure 6(*b*)). This drop in coherence is first evident in the coherence pair spanning 17 August 2003 through 10 September 2003 when the coherence for burn site 1 dropped to about 0.25 (± 0.08 SD). Burn site 2 first lost coherence in the 17 August 2003 to 4 October 2003 pair, when the coherence dropped to about 0.3 (± 0.06 SD).

4.2 Analysis of post-fire data

For post-fire radar acquisitions, the backscattered intensity levels for the 15 December 2003 image dropped to very low intensity levels of –13 dB (1.00 SD) for burn site 1 and –15 dB (0.70 SD) for burn site 2 and remained at very low levels during the 18 January 2004 acquisition (figures 6(*a*)). However, during the two winter acquisitions, burn site 2 experienced the largest drop in intensity levels of about 15 dB, burn site 1 dropped about 9 dB, and the unburned site only dropped about 4 dB. This drop in intensity in the winter images is probably because of the presence of ice/snow and because the ice/snow affects the burned sites more than the unburned site. Our post-fire analysis for the summer of 2004 is based on four images acquired in June, July, August and September (figures 5(*n*–*q*) and 6(*b*)). For burn site 1, the backscatter intensity characteristics returned from their low winter levels to about –8 dB (1.44 SD) in June 2004 and further increased to about –5 dB (1.53 SD) during the August 2004 acquisition (figure 6(*a*) line c). This 3 dB intensity increase is contrary to the normal seasonal drop in intensity that is caused by a drying of the top soil layers and is probably caused by increased melting of the active layer. The first post-fire 2004 coherence pair from 24 June 2004 through 4 September 2004 shows that while burn site 1 remains incoherent throughout the duration of the study, burn site 2 returned to high, pre-fire coherence levels (figure 6(*b*) line c).

4.3 Discussion

Since no ground-truth data are available for the fire, the NLCD and NBR data will help us analyse the effects of the 2003 B346 wildfire on the boreal landscape, and the

NLCD dataset will also provide information related to pre-fire vegetation structure. According to the NLCD vegetation database, both burn sites 1 and 2 have a woody vegetation type (figure 2(*b*)). Typically, the primary radar interaction type for woody
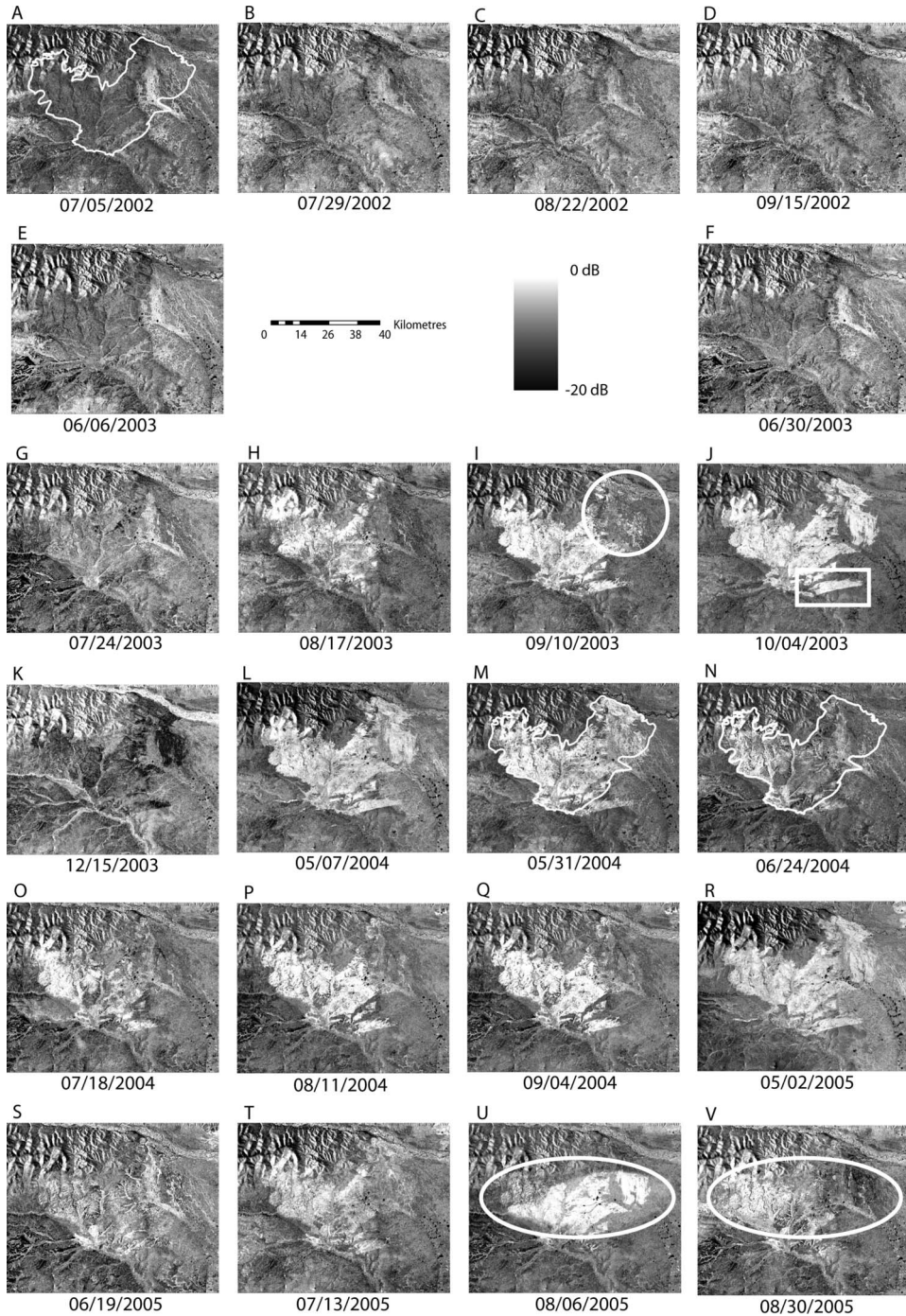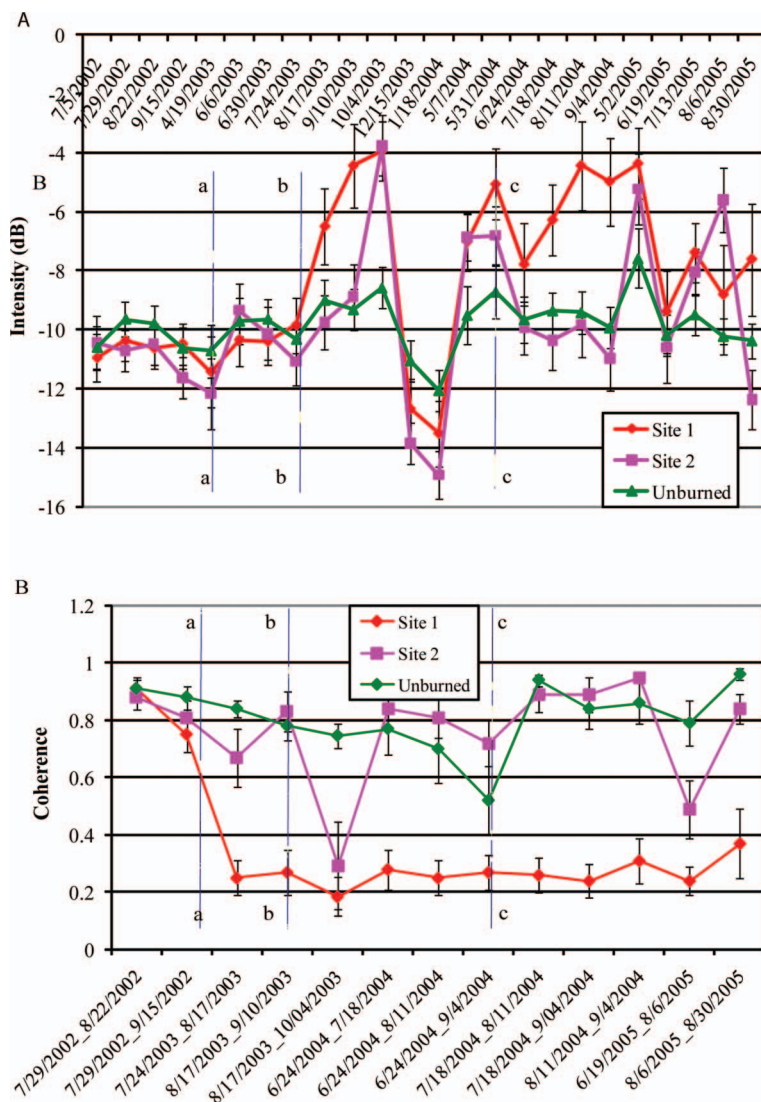
Figure 6. Temporal profiles of the three study sites on the SAR intensity (A) and coherence (B) data. The data presented here depict the average intensity and coherence data, and the whisker in the two temporal profiles indicates one standard deviation from the mean of the study site and date. Lines A, B, and C in the profiles are discussed in the text.

Figure 5. All Radarsat-1 intensity images acquired from the B346 fire except for three winter scenes are presented here. The boundary of the B346 fire, as delineated by the Bureau of Land Management, Alaska Fire Service is transposed on A, M, and N. Pre-fire Radarsat-1 scenes (A–F), during the fire (G–J), and post-fire (K–V) intensity images show the temporal effects of the B346 fire on the Radatsat-1 backscattered intensity return. The unusually strong intensity return in the 6 August 2005 image is due to a 2005 fire that occurred on the western edge of the B346 fire and atmospheric/rain contamination in the eastern part of the study area. The finding of atmospheric contamination or rain is supported by the two coherence pairs that use that image.
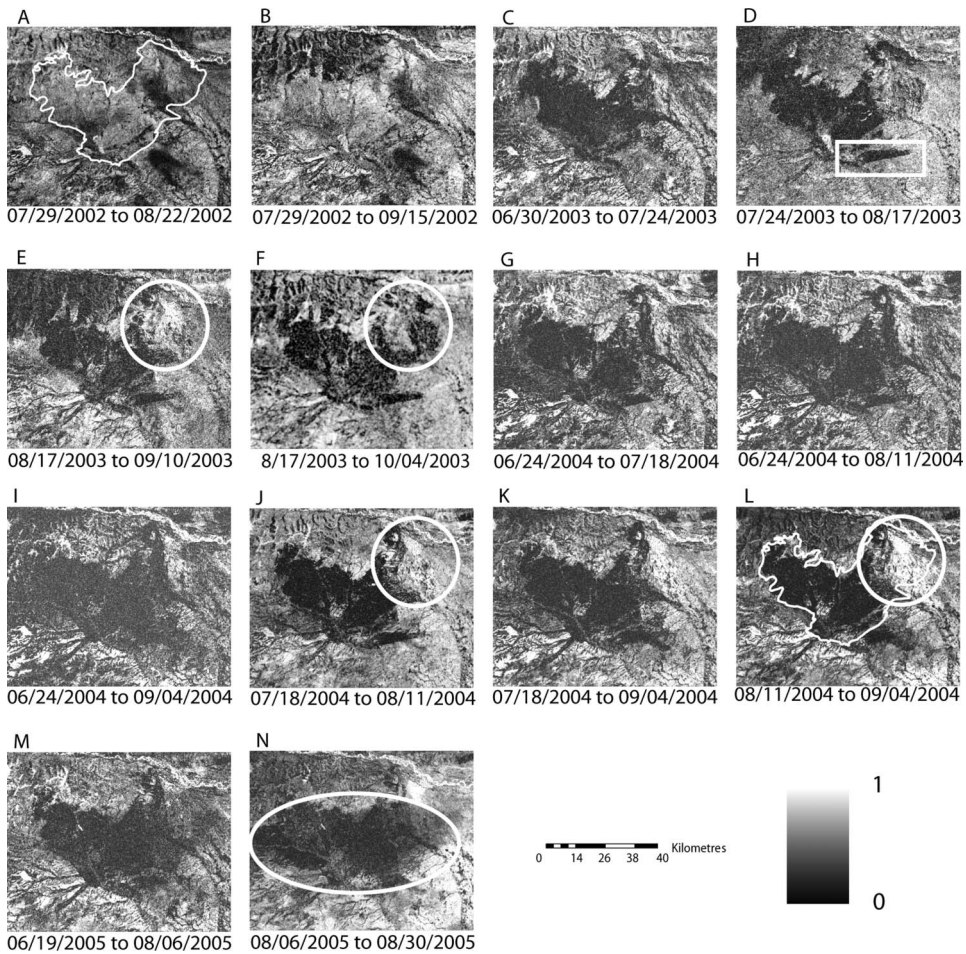
Figure 7. Radarsat-1 coherence estimates for the 2003 B346 fire. The coherence images show the effects of the fire between two observation periods. For example, the north-northeast part of the fire (white circled area in E, F, J and L) regained coherence in the 2004 image, while the main body of the fire remains incoherent throughout the period of observation. The image acquired on 6 August 2005 appears to be contaminated by atmospheric or other environment effects; both coherence pairs using the scene show areas of low coherence outside the fire boundary (white ellipse in N).

vegetation is volumetric scattering. Given an increase in intensity of about 6 dB, we deduce that much of the vegetation canopy was consumed by the fire. Before the fire, the vegetation canopy of the boreal forest exhibited volumetric scattering, while radar interactions are dominated by surface scattering and double-bounce interactions during and after the fire. But why did the intensity levels for burn site 1 remain elevated throughout the study while the intensity levels for burn site 2 returned to near normal levels? For the intensity signal for burn site 1 to remain bright after the fire the surface of the site must be rough with respect to the wavelength of the radar. Conversely, the surface of burn site 2 must be very smooth with respect to the wavelength of the Radarsat-1 SAR system. If the surface for site 1 is littered with debris we would expect higher than normal intensity returns. The

opposite is also true for burn site 2. From the elevation data in figure 2(*a*), we can see that burn site 2 is located in a topographically flat area while the topography for burn site 1 is more variable. According to Duffy *et al*. (2007), fires in topographically diverse areas such as burn site 1 tend to be less severely burned than fires occurring in flat, less topographically diverse areas. Inspection of the dNBR (22 August 2002 to 14 August 2005; figure 3(*c*)) data for burn sites 1 and 2 suggests that burn site 2 (dNBR 315; SD $\pm$ 53) may have been more severely burned than burn site 1 (dNBR $\sim$267, SD 60). From the dNBR data we suggest that burn site 2 is probably more severely burned than burn site 1 and that the surface of burn site 1 is laden with a large amount of debris that is rough with respect to the radar's C-band wavelength. One question remains: why did the post-fire coherence levels for burn site 1 remain at very low levels while its intensity values remained elevated? For coherence levels at burn site 1 to remain very low ($\sim$0.3) throughout the duration of the study, environmental changes at the scale of the 5.7 cm Radarsat-1 wavelength must continue to occur (figure 6(*b*)). Additionally, these changes must be enough to cause a loss of coherence over the shortest possible observation periods (24 days). Using the intensity and NLCD datasets, we determined that the primary scattering mechanism for burn site 1 was surface/double-bounce scattering because of the consumption of the vegetation canopy. For the low coherence to continue subsequent to the fire, the spatial orientation of the debris deposits must change significantly over time. The loss of insulation provided by the partial burning of the duff layer can lead to increased thawing of the active layer and increased soil moisture. The intensity and coherence profiles for burn site 1 are the profiles for a moderately burned forest. The presence of dead vegetation on the surface combined with higher than normal soil moisture levels and Radarsat-1's propensity for double-bounce scattering explains the much higher than normal intensity levels for burn site 1. The increased thawing of the active layer for burn site 1 increases soil moisture levels and creates conditions necessary for enhanced amounts of soil creep. Soil creep with the natural downslope movement of dead surface vegetation explains the very low coherence levels for burn site 1. With little dead vegetation on the surface and higher soil moisture levels, we would expect that burn site 2 would return to near normal intensity levels and be very coherent. These observations are consistent with the dNBR results that burn site 2 had a higher burn severity than burn site 1.

5. Conclusion

With a 24-day repeat pass frequency, the intensity and coherence data from the C-band Radarsat-1 system provided an unprecedented view of the 2003 B346 wildfire located in the Yukon Flats National Wildlife Refuge, Alaska. The Radarsat-1 data allowed us to more accurately delineate the boundary of the fire and map the progression of the fire over its duration. We found that the B346 fire started in the foothills of the Phillip Smith Mountains shortly before the acquisition of the 24 July 2003 scene, proceeded to the south southeast towards the Yukon Flats, then moved in a northeasterly direction. For our analysis of the B346 fire, we subset three small test sites, two from within the fire and one undisturbed control site. The B346 fire increased backscatter intensity levels at burned areas from pre-fire background levels of about –11 dB to maximum intensity levels of about –4 dB. During-fire coherence values experienced a similar drop from 0.8 to about 0.3, coinciding with the burning of the boreal vegetation. Using the Radarsat-1 intensity, coherence, and NBR data,

we conclude that burn site 2 experienced higher burn severity than that observed at burn site 1 and that the surface of burn site 1 is laden with debris. Our research shows that Radarsat-1 intensity and coherence estimates are sensitive to burn severity within a boreal forested area and that each data type provides unique information related to the fire.

Acknowledgements

References

ABBOTT, K.N., LEBLON, B., STAPLES, G.C., MACLEAN, D.A. and ALEXANDER, M.E., 2007, Fire danger monitoring using Radarsat-1 over northern boreal forests. *International Journal of Remote Sensing*, **28**, pp. 1317–1338.

BAMLER, R. and HARTL, P., 1998, Synthetic aperture radar interferometry. *Inverse Problems*, **14**, pp. R1–54.

BONAN, G.B. and SHUGART, H.H., 1989, Environmental factors and ecological processes in boreal forests. *Annual Review of Ecology and Systematics*, **20**, pp. 1–28.

BOURGEAU-CHAVEZ, L.L., HARRELL, P.A., KASISCHKE, E.S. and FRENCH, N.F., 1997, The detection and mapping of Alaskan wildfires using a spaceborne imaging radar system. *International Journal of Remote Sensing*, **18**, pp. 355–373.

BOURGEAU-CHAVEZ, L.L., KASISCHKE, E.S. and RUTHERFORD, M.D., 1999, Evaluation of ERS SAR data for prediction of fire danger in a boreal region. *International Journal of Wildland Fire*, **9**, pp. 183–194.

BOURGEAU-CHAVEZ, L.L., KASISCHKE, E.S., BRUNZELL, S., MUDD, J.P. and TUKMAN, M., 2002, Mapping fire scars in global boreal forests using imaging radar data. *International Journal of Remote Sensing*, **23**, pp. 4211–4234.

BOURGEAU-CHAVEZ, L.L., KASISCHKE, E.S., RIORDAN, K., BRUNZELL, S., NOLAN, M., HYER, E., SLAWSKI, J., MEDVECZ, M., WALTERS, T. and AMES, S., 2007, Remote monitoring of spatial and temporal surface soil moisture in fire disturbed boreal forest ecosystems with ERS SAR imagery. *International Journal of Remote Sensing*, **28**, pp. 2133–2162.

CURLANDER, J. and MCDONOUGH, R., 1991, *Synthetic Aperture Radar Systems and Signal Processing* (New York: John Wiley and Sons).

DOBSON, C.M., ULABY, F.T. and PIERCE, L.E., 1995, Land-cover classification and estimation of terrain attributes using synthetic aperture radar. *Remote Sensing of Environment*, **51**, pp. 199–214.

DUFFY, P.A., EPTING, J., GRAHAM, J.M., RUPP, T.S. and MCGUIRE, A.D., 2007, Analysis of Alaskan burn severity patterns using remotely sensed data. *International Journal of Wildland Fires*, **16**, pp. 277–284. DOI: 10.1071/WF06034.

FRENCH, H.F., BOURGEAU-CHAVEZ, L.L., WANG, Y. and KASISCHKE, E.S., 1999, Initial observations of Radarsat-1 imagery at fire-disturbed sites in interior Alaska. *Remote Sensing of Environment*, **68**, pp. 89–94.

GESCH, D., 1994, Topographic Data Requirement for EOS, Global Change Research. US Geological Survey Open File Report 94-626.

GILLETT, N.P., WEAVER, A.J., ZWIERS, F.W. and FLANNIGAN, M.D., 2004, Detecting the effect of climate change on Canadian forest fires. *Geophysical Research Letters*, **31**, p. L18211. DOI: 10.029/2004GL020876.

HAGBERG, J.O., ULANDER, L.M.H. and ASKNE, J., 1995, Repeat-pass SAR interferometry over forested terrain. *IEEE Transactions on Geoscience and Remote Sensing*, **33**, pp. 331–339.

HENDERSON, F.M. and LEWIS, A.J., 1998, *Manual of Remote Sensing: Principles and applications of imaging radar* (New York: John Wiley & Sons).

HOMER, C., HUANG, C., YANG, L. and WYLIE, B.K., 2004, Development of a 2001 National Land-Cover Database for the United States. *Photogrammetric Engineering and Remote Sensing*, **70**, pp. 829–840.

HOMER, C., DEWITZ, J., FRY, J., COAN, M., HUSSAIN, N., LARSON, C., HEROLD, N., MCKERROW, A., VANDRIEL, J.N. and WICKHAM, J., 2007, Completion of the 2001 National Land Cover Database for the conterminous United States. *Photogrammetric Engineering and Remote Sensing*, **73**, pp. 337–341.

JOHNSTONE, J.F. and CHAPIN, F.S., 2006, Effects of soil burn severity on post-fire tree recruitment in boreal forests. *Ecosystems*, **9**, pp. 14–31. DOI: 10.1007/s10021-004-0042-x.

KASISCHKE, E.S. and FRENCH, N.H., 1995, Locating and estimating the areal extent of wildfires in Alaskan boreal forests using multiple-season AVHRR NDVI composite data. *Remote Sensing of Environment*, **51**, pp. 263–275.

KASISCHKE, E.S. and JOHNSTONE, J.F., 2005, Variation in postfire organic layer thickness in a black spruce forest complex in interior Alaska and its effects on soil temperature and moisture. *Canadian Journal of Forest Research*, **35**, pp. 2164–2177. DOI: 10.1139/X05-159.

KASISCHKE, E.S. and TURETSKY, M.R., 2006, Recent change in the fire regime across the North American boreal region – spatial and temporal patterns of burning across Canada and Alaska. *Geophysical Research Letters*, **33**, p. L09703. DOI: 10.10292006GL025677.

KASISCHKE, E.S., BOURGEAU-CHAVEZ, L.L. and JOHNSTONE, J.F., 2007, Assessing spatial and temporal variations in surface soil moisture in fire-disturbed black spruce forests in Interior Alaska using spaceborne synthetic aperture radar imagery – implications for post-fire tree recruitment. *Remote Sensing of Environment*, **108**, pp. 42–58.

KEY, C.H. and BENSON, N.C., 2006, FIREMON: Fire effects monitoring and inventory system. Landscape assessment: sampling and analysis methods. Technical Report RMRS-GTR-164-CD, US Forest Service Rocky Mountain Research Station.

KWOUN, O., LU, Z. and RYKHUS, R.P., 2006, Analysis of SAR backscattering variations and InSAR derived water-level changes over swamp forests, southeastern Louisiana. In *IEEE International Geoscience and Remote Sensing Symposium and 27th Canadian Symposium on Remote Sensing* (Denver, CO: IEEE Geoscience and Remote Sensing Society).

LANDHAUSSER, S.M. and WEIN, R.W., 1993, Vegetation recovery and tree establishment at the Arctic treeline: climate-change-vegetation-response hypothesis. *The Journal of Ecology*, **81**, pp. 665–672.

LEBLON, B., KASISCHKE, E., ALEXANDER, M., DOYLE, M. and ABBOTT, M., 2002, Fire danger monitoring using ERS-1 SAR images in the case of northern boreal forests. *Natural Hazards*, **27**, pp. 231–255.

LEE, J.-S., 1986, Speckle supression and analysis for synthetic aperature radar images. *Optical Engineering*, **25**, pp. 636–643.

LEVINSON, D., 2004, Climate of 2004 Wildfire Season Summary. NOAA/National Climate Data Center. http://www.ncdc.noaa.gov/oa/climate/research/2004/fire04.html

LU, Z., CRANE, M., KWOUN, O.-I., WELLS, C., SWARZENSKI, C. and RYKHUS, R., 2005a, C-band radar observes water level change in swamp forests. *EOS Transactions, American Geophysical Union*, **86**, pp. 141–144.

LU, Z., WICKS, C., KWOUN, O., POWER, J.A. and DZURISIN, D., 2005b, Surface deformation associated with the March 1996 earthquake swarm at Akutan Island, Alaska, revealed by C-band ERS and L-band JERS radar interferometry. *Canadian Journal of Remote Sensing*, **31**, pp. 7–20.

LU, Z., DZURISIN, D., WICKS, C., POWER, J., KWOUN, O., and RYKHUS, R., 2007, Diverse
    deformation patterns of Aleutian volcanoes from satellite interferometric synthetic
    aperture radar (InSAR). In *Volcanism and Subduction: The Kamchatka Region*, J.
    Eichelberger, E. Gordeev, M. Kasahara, P. Izbekov and Jonathan Lees (Eds),
    American Geophysical Union Monograph Series 172. Washington, D.C.: AGU, pp.
    249–261.
LUTES, D.C., KEANE, R.E., CARATTI, J.F., KEY, C.H., BENSON, N.C., SUTHERLAND, S. and
    GANGI, L.J., 2006, FIREMON: Fire effects monitoring and inventory system. United
    States Department of Agriculture Forest Service, Rocky Mountain Research Station.
MASSONNET, D. and FEIGL, K., 1998, Radar interferometry and its application to changes in
    the Earth's surface. *Reviews of Geophysics*, **36**, pp. 441–500.
O'NEAL, K.P., RICHTER, D.D. and KASISCHKE, E.S., 2006, Succession-driven change in soil
    respiration following fire in black spruce stands of interior Alaska. *Biogeochemistery*,
    80, pp. 1–20. DOI: 10.107/s10533-005-5964-7.
RAMSEY, E.I., LU, Z., RANGOONWALA, A. and RYKHUS, R., 2006, Multiple baseline radar
    interferometry applied to coastal land cover classification and change analysis.
    GIScience & Remote Sensing, **43**, pp. 283–309.
RYKHUS, R., 2009, Personal communication with Z. Zhu.
ULABY, F.T., MOORE, R.K., and FUNG, A.K., 1986, *Microwave Remote Sensing: Active and
    passive* (Boston, MA: Artech House.
VOGELMAN, J.E., HOWARD, S.M., YANG, L., LARSON, C.R., WYLIE, B.K. and VANDRIEL, J.N.,
    2001, Completion of the 1990's National Land Cover Dataset for the conterminous
    United States from Landsat TM and ancillary data sources. *Photogrammetric
    Engineering and Remote Sensing*, **67**, pp. 650–662.
WEGMULLER, U., 1990, The effect of freezing and thawing on the microwave signatures of bare
    soil. *Remote Sensing of Environment*, **33**, pp. 123–135.
ZEBKER, H. and VILLASENOR, J., 1992, Decorrelation in interferometric radar echoes. *IEEE
    Transactions on Geoscience and Remote Sensing*, **30**, pp. 950–959.